

Kondo effect in asymmetric Josephson couplings through a quantum dot

Yoshihide Tanaka¹, Akira Oguri¹, and A. C. Hewson²

¹*Department of Material Science, Osaka City University, Sumiyoshi-ku, Osaka 558-8585, Japan*

²*Department of Mathematics, Imperial College, 180 Queen's Gate, London SW7 2BZ, UK*

(Dated: September 13, 2018)

Asymmetry in the Josephson couplings between two superconductors through a quantum dot is studied based on a single impurity Anderson model using the numerical renormalization group (NRG). Specifically, we examine how the difference between the couplings Γ_L and Γ_R affects the ground state, which is known to show a quantum phase transition between a nonmagnetic singlet and a magnetic doublet depending on the various parameters; the Coulomb interaction U , onsite potential ϵ_d , level width Γ_ν caused by the hybridization, and superconducting gap $\Delta_\nu \equiv |\Delta_\nu|e^{i\theta_\nu}$ for the leads on the left and right ($\nu = L, R$). Our results show that whether the local moment is fully screened or not depends substantially on the asymmetry in the couplings $\Gamma_L \neq \Gamma_R$. It tends to make the singlet ground state stable, while the amplitude $|\Delta_\nu|$ and phase difference $\phi \equiv \theta_R - \theta_L$ of the superconducting gaps tend to suppress the screening. We also discuss some general symmetry properties of the system and their relation to the current conservation.

PACS numbers: 72.10.-d, 72.10.Bg, 73.40.-c

I. INTRODUCTION

The Kondo effect in superconductors has been studied over three decades.^{1,2,3,4} It was shown in early years that the competition between the superconducting (SC) gap and Kondo energy scale T_K determines the low-temperature properties. The SC energy gap Δ_{SC} disturbs the conduction-electron screening of the local moment. The ground state becomes a magnetic doublet for $\Delta_{SC} \gg T_K$, while the ground state is still a nonmagnetic singlet for $\Delta_{SC} \ll T_K$. These aspects of the Kondo physics in superconductors have been re-examined precisely by efficient numerical methods such as the quantum Monte Carlo (QMC)⁵ and numerical renormalization group (NRG) approaches.^{6,7,8,9}

In quantum dots embedded in a Josephson junction, new interesting features have been predicted to be observed^{10,11,12} and some experiments have been reported.^{13,14,15,16} Particularly, the screening of the local moment in the quantum dot is affected not only by the size of the two SC gaps but also by the Josephson phase ϕ between the two SC leads on the left and right. The phase difference ϕ also induces the Josephson current flowing through the dot. It can drive a quantum phase transition (QPT) between the singlet and doublet ground states, and at the critical point the direction of the current changes discontinuously.

These properties of the SC-dot-SC systems have been studied with various theoretical approaches; such as the noncrossing approximation,^{17,18} slave-boson mean-field theory,^{19,20} perturbation theory in the Coulomb interaction U ,²¹ QMC,^{22,23} and NRG.^{24,25} So far, however, most of the calculations have been carried out assuming a highly symmetric condition as $|\Delta_L| = |\Delta_R|$ and $\Gamma_L = \Gamma_R$.^{17,18,19,20,21,22,24} Here, $\Delta_\nu \equiv |\Delta_\nu|e^{i\theta_\nu}$ is the SC gap of the leads on the left and right ($\nu = L, R$), and Γ_ν is the bare level width due to the hybridization. Therefore, the feature of the QPT far from the symmetric

condition is one of the theoretical issues to be clarified with some accurate approaches.

In a previous work, we have studied the ground-state properties in the case of $|\Delta_L| \neq |\Delta_R|$. In real quantum dots, it corresponds to the situation that the two superconductors connected to the dot are not identical.²⁵ Specifically, we have considered the limit where one of the two SC gaps, Δ_L , is much larger than the other one Δ_R . In the limit of $|\Delta_L| \rightarrow \infty$, the left lead has been shown to be separated from the rest of the system, which consists of the dot and right lead. It just leaves a static SC pair potential, which is given by $\Delta_d = \Gamma_L e^{i\theta_L}$, in the dot. The pair potential appears because a SC proximity from the left lead is allowed even in the large gap limit, while the quasi-particle tunneling into the left lead is prohibited. This situation is described by a single-channel Anderson model with an extra SC pair potential Δ_d in the impurity site. The simplified model possesses essential ingredients of the Kondo and Josephson effects, and the phase difference $\phi \equiv \theta_R - \theta_L$ can be defined between Δ_d and Δ_R . We have studied the features of QPT applying the NRG to this model, and have confirmed, for example, that the Andreev bound state emerging close to the Fermi level causes a re-entrant QPT near half-filling for $\phi \simeq \pi$ and $\Gamma_L \simeq \Gamma_R$.²⁵

Another aspect that seems to be important is how the asymmetry in the couplings Γ_L and Γ_R affects QPT. That is the main subject of the present work. The SC proximity effect depends strongly on the environment surrounding the dot, and the competition between the Kondo and proximity effects determine the low-energy properties. In this paper we present the results of the QPT phase diagram obtained for the asymmetric couplings $\Gamma_L \neq \Gamma_R$. The NRG calculations have been carried out mainly using the two-channel model, assuming the two gaps are equal in size $|\Delta_L| = |\Delta_R|$. Our results show that the asymmetry in the couplings tends to enhance the screening of the local moment.

The model and some symmetry properties of the Anderson impurity in the Josephson junctions are described in Sec. II, based on a rotational symmetry in the pseudo-spin space. The NRG approach and the results of the phase diagram for QPT obtained in some typical parameter regions are discussed in Sec. III. We also discuss in Sec. IV the roles of the asymmetry in two solvable cases: noninteracting case $U = 0$, and a superconducting version of the atomic limit for $|\Delta_L| \rightarrow \infty$ and $|\Delta_R| \rightarrow \infty$ which can also be considered as one of the fixed points of NRG. A summary is given in Sec. V. We also describe some general properties deduced from the current conservation in the appendix.

II. MODEL FOR A SC-DOT-SC JUNCTION

We describe in this section the model and some of the symmetry properties. Specifically, at half-filling for the Josephson junctions with $\phi = 0$ or π , the system has a global U(1) symmetry in a pseudo-spin space. It enables us to map the SC leads onto the normal conductors with a staggered potential, as shown by Satori *et al.*⁶

A. General formulation

We start with a single Anderson impurity connected to two SC leads on the left (L) and right (R), as illustrated in Fig. 1. The Hamiltonian is given by

$$\mathcal{H} = \mathcal{H}_d^0 + \mathcal{H}_d^U + \mathcal{H}_T + \mathcal{H}_c^0 + \mathcal{H}_c^{\text{SC}}, \quad (1)$$

$$\mathcal{H}_d^0 = \xi_d (n_d - 1), \quad \mathcal{H}_d^U = \frac{U}{2} (n_d - 1)^2, \quad (2)$$

$$\mathcal{H}_T = \sum_{\nu=L,R} \sum_{\sigma} v_{\nu} \left(c_{\nu,0\sigma}^{\dagger} d_{\sigma} + d_{\sigma}^{\dagger} c_{\nu,0\sigma} \right), \quad (3)$$

$$\mathcal{H}_c^0 = \sum_{\nu=L,R} \sum_{n=0}^{\infty} \sum_{\sigma} t_{\nu,n} \left(c_{\nu,n+1\sigma}^{\dagger} c_{\nu,n\sigma} + c_{n,\nu\sigma}^{\dagger} c_{\nu,n+1\sigma} \right), \quad (4)$$

$$\mathcal{H}_c^{\text{SC}} = \sum_{\nu=L,R} \sum_{n=0}^{\infty} \left(\Delta_{\nu} c_{\nu,n\uparrow}^{\dagger} c_{\nu,n\downarrow}^{\dagger} + \Delta_{\nu}^* c_{\nu,n\downarrow} c_{\nu,n\uparrow} \right). \quad (5)$$

Here, $\xi_d \equiv \epsilon_d + U/2$, with ϵ_d the impurity level, and U is the onsite Coulomb interaction. The operator d_{σ}^{\dagger} creates an electron with spin σ at the impurity site, and $n_d = \sum_{\sigma} d_{\sigma}^{\dagger} d_{\sigma}$. The other operator $c_{\nu,0\sigma}$ annihilates a conduction electron that couples directly to the dot via the tunneling matrix element v_{ν} . The electrons in the leads can be described by the Hamiltonian of a tight-binding form without loss of generalities.²⁹ The hopping matrix element $t_{\nu,n}$ determines a continuous one-particle spectrum $\epsilon_{k\nu}$ and eigenfunction $\varphi_{k\nu}(n)$, by which the hybridization strength can be written in the form $\Gamma_{\nu}(\epsilon) = \pi v_{\nu}^2 \sum_k |\varphi_{k\nu}(0)|^2 \delta(\epsilon - \epsilon_{k\nu})$.

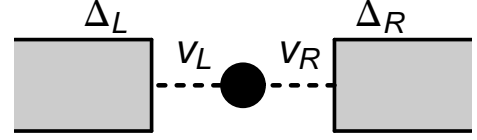


FIG. 1: Schematic picture of an Anderson impurity connected to two SC leads with the gaps Δ_L and Δ_R , where v_L and v_R are the tunneling matrix elements.

The symmetry properties of the system can be clearly seen, in the Nambu representation using the spinors

$$\psi_d = \begin{bmatrix} d_{\uparrow} \\ d_{\downarrow}^{\dagger} \end{bmatrix}, \quad \psi_{\nu,n} = \begin{bmatrix} c_{\nu,n\uparrow} \\ (-1)^{n+1} c_{\nu,n\downarrow}^{\dagger} \end{bmatrix}. \quad (6)$$

Then, eqs. (2)–(5) can be rewritten in the form

$$\mathcal{H}_d^0 = \xi_d \psi_d^{\dagger} \tau_3 \psi_d, \quad \mathcal{H}_d^U = \frac{2U}{3} \vec{i}_d \cdot \vec{i}_d, \quad (7)$$

$$\mathcal{H}_T = \sum_{\nu=L,R} v_{\nu} \left(\psi_{\nu,0}^{\dagger} \psi_d + \psi_d^{\dagger} \psi_{\nu,0} \right), \quad (8)$$

$$\mathcal{H}_c^0 = \sum_{\nu=L,R} \sum_{n=0}^{\infty} t_{\nu,n} \left(\psi_{\nu,n+1}^{\dagger} \psi_{\nu,n} + \psi_{\nu,n}^{\dagger} \psi_{\nu,n+1} \right), \quad (9)$$

$$\mathcal{H}_c^{\text{SC}} = \sum_{\nu=L,R} \sum_{n=0}^{\infty} (-1)^{n+1} \psi_{\nu,n}^{\dagger} \Delta_{\nu} \psi_{\nu,n}. \quad (10)$$

Here, Δ_{ν} and \vec{i}_d are defined by

$$\Delta_{\nu} = \begin{bmatrix} 0 & \Delta_{\nu} \\ \Delta_{\nu}^* & 0 \end{bmatrix}, \quad \vec{i}_d = \frac{1}{2} \psi_d^{\dagger} \vec{\tau} \psi_d, \quad (11)$$

and τ_k for $k = 1, 2, 3$ is the Pauli matrix. The Coulomb interaction \mathcal{H}_d^U is isotropic in the pseudo-spin space, and the expression given in eq. (7), which is identical to that in eq. (2), explicitly shows the rotational symmetry. Furthermore, the current through the dot can be expressed in the form,

$$J_R = -i \frac{e v_R}{\hbar} \left(\psi_{R,0}^{\dagger} \tau_3 \psi_d - \psi_d^{\dagger} \tau_3 \psi_{R,0} \right), \quad (12)$$

$$J_L = -i \frac{e v_L}{\hbar} \left(\psi_d^{\dagger} \tau_3 \psi_{L,0} - \psi_{L,0}^{\dagger} \tau_3 \psi_d \right). \quad (13)$$

The current is conserved such that $\partial n_d / \partial t + J_R - J_L = 0$, as described also in the appendix A.

The rotational symmetry in the pseudo-spin space are described by the operator

$$\vec{I} = \vec{i}_d + \frac{1}{2} \sum_{\nu=L,R} \sum_{n=0}^{\infty} \psi_{\nu,n}^{\dagger} \vec{\tau} \psi_{\nu,n}. \quad (14)$$

The z component corresponds to the half of the total charge $Q = 2I_z$, and I_x (I_y) represents the real (imaginary) part of the SC pair potentials. These three components satisfy the same commutation relations as that

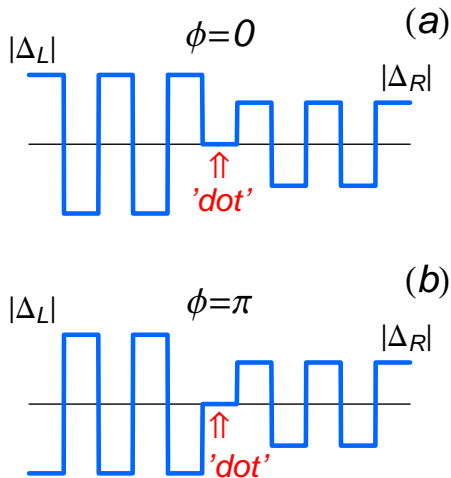


FIG. 2: Potential profiles for the quasi-particles $\gamma_{\nu,n\sigma}$, given in eqs. (16)–(20), for the Josephson junctions with (a) $\phi = 0$, and (b) $\phi = \pi$, at half-filling $\xi_d = 0$. The Horizontal line corresponds to the Fermi level.

of the angular momentums,

$$[I_x, I_y] = i I_z, \quad [I_y, I_z] = i I_x, \quad [I_z, I_x] = i I_y. \quad (15)$$

In the pseudo-spin space, the onsite potential ξ_d can be interpreted as a local external field along the z axis, and the SC gaps Δ_ν can be regarded as a staggered field in the x - y plane. Therefore, if $\xi_d = 0$ and $\Delta_\nu = 0$, which corresponds to normal leads in the particle-hole symmetric case, the system has a full rotational symmetry in the pseudo-spin space as well as the rotational symmetry in the real spin space, because $[I_k, \mathcal{H}] = 0$ for $k = x, y, z$.

Another typical case is that of the Josephson junction $\Delta_\nu \neq 0$ with the particle-hole symmetry $\xi_d = 0$. In this case the z component of the external field vanishes. Therefore, if we take the quantization axis to be in the y -direction by carrying out a spinor rotation of $\pi/2$ with respect to the x axis, the Hamiltonian \mathcal{H} takes a real symmetric form. Then, with the new axis, the current operators are described by a Pauli matrix τ_2 instead of τ_3 in eqs. (12) and (13).

B. Particle-Hole symmetric case with real gaps

The two SC gaps Δ_L and Δ_R are essentially real for the Josephson junctions with $\phi = 0$ or π . In this case, if the system also has the particle-hole symmetry $\xi_d = 0$, the model can be mapped onto a normal asymmetric Anderson model with a staggered potential.⁶ It is owing to a conservation associated with $[I_x, \mathcal{H}] = 0$, caused by a U(1) symmetry along the x axis. It enables us to transform I_x into the total number of the quasi-particles as shown in eq. (21). This feature can be seen explicitly

if we take the quantization axis to be in the x direction,⁶ carrying out a spinor rotation of $\pi/2$ with respect to the y axis by a unitary transform $e^{i\frac{\pi}{4}\tau_2}$ as

$$\begin{bmatrix} \gamma_{-1\uparrow} \\ \gamma_{-1\downarrow}^\dagger \end{bmatrix} = \begin{bmatrix} \frac{1}{\sqrt{2}} & \frac{1}{\sqrt{2}} \\ -\frac{1}{\sqrt{2}} & \frac{1}{\sqrt{2}} \end{bmatrix} \psi_d, \quad \begin{bmatrix} \gamma_{\nu,n\uparrow} \\ \gamma_{\nu,n\downarrow}^\dagger \end{bmatrix} = \begin{bmatrix} \frac{1}{\sqrt{2}} & \frac{1}{\sqrt{2}} \\ -\frac{1}{\sqrt{2}} & \frac{1}{\sqrt{2}} \end{bmatrix} \psi_{\nu,n}. \quad (16)$$

Then, the Hamiltonian can be expressed in the form

$$\mathcal{H}_d^U = \frac{U}{2} \left(\sum_\sigma \gamma_{-1\sigma}^\dagger \gamma_{-1\sigma} - 1 \right)^2, \quad (17)$$

$$\mathcal{H}_T = \sum_\sigma v_\nu \left(\gamma_{\nu,0\sigma}^\dagger \gamma_{-1\sigma} + \gamma_{-1\sigma}^\dagger \gamma_{\nu,0\sigma} \right), \quad (18)$$

$$\mathcal{H}_c^0 = \sum_{\nu=L,R} \sum_{n=0}^{\infty} \sum_\sigma t_{\nu,n} \left(\gamma_{\nu,n+1\sigma}^\dagger \gamma_{\nu,n\sigma} + \gamma_{\nu,n\sigma}^\dagger \gamma_{\nu,n+1\sigma} \right), \quad (19)$$

$$\mathcal{H}_c^{\text{SC}} = \sum_{\nu=L,R} \sum_{n=0}^{\infty} (-1)^{n+1} \Delta_\nu \left(\sum_\sigma \gamma_{\nu,n\sigma}^\dagger \gamma_{\nu,n\sigma} - 1 \right). \quad (20)$$

Note that $\mathcal{H}_d^0 = 0$, because of the particle-hole symmetry, $\xi_d = 0$. Therefore, the energy spectrum is determined by the quasi-particles, the total number of which is conserved

$$2I_x = q_{-1} + \sum_{\nu=L,R} \sum_{n=0}^{\infty} \left(\sum_\sigma \gamma_{\nu,n\sigma}^\dagger \gamma_{\nu,n\sigma} - 1 \right), \quad (21)$$

$$q_{-1} \equiv \sum_\sigma \gamma_{-1\sigma}^\dagger \gamma_{-1\sigma} - 1 = d_\downarrow^\dagger d_\uparrow + d_\uparrow^\dagger d_\downarrow. \quad (22)$$

Particularly, the local charge q_{-1} corresponds to the SC pair correlation penetrated into the impurity site. The profile of the potential that the quasi-particles feel is illustrated in Fig. 2. For the Josephson junction with $\phi = 0$ the potential still shows a regular staggered period around the dot, while for $\phi = \pi$ the steps of the potential changes like that in a defect, or dislocation. The potential profile suggests that the SC proximity effect, which causes a finite anomalous average $\langle q_{-1} \rangle$, is larger for $\phi = 0$ than that in the case of π . The penetration of the SC correlations into the impurity site depends on the tunneling strength Γ_ν and the size of the SC gaps Δ_ν . Specifically, for $\phi = \pi$ and $\Gamma_R = \Gamma_L$, the impurity level evolves to the Andreev bound state emerging just on the Fermi level situated in the middle of the energy gap. In this case, if also the size of the two gaps are equal $|\Delta_R| = |\Delta_L|$, the SC correlations cancel out $\langle q_{-1} \rangle = 0$ in the impurity site. It also holds in the particle-hole asymmetric case $\xi_d \neq 0$ as shown in the appendix A based on the current conservation.

C. Particle-Hole asymmetric case for $\phi = \pi$

There is a different symmetry for a π -junction $\phi = \pi$, in the case of $\Gamma_R = \Gamma_L$ and $|\Delta_R| = |\Delta_L|$. It holds without

the particle-hole symmetry, and reveals, for instance, in the Nambu form of the Green's function \mathbf{G} given in eq. (A12) in the appendix A. The underlying symmetry links to the conservation of a channel charge Q_{ch} defined by

$$Q_{\text{ch}} = n_d + \sum_{n=0}^{\infty} \sum_{\sigma} (a_{n\sigma}^{\dagger} a_{n\sigma} - b_{n\sigma}^{\dagger} b_{n\sigma}),$$

$$a_{n\sigma} = \frac{c_{R,n\sigma} + c_{L,n\sigma}}{\sqrt{2}}, \quad b_{n\sigma} = \frac{c_{R,n\sigma} - c_{L,n\sigma}}{\sqrt{2}}. \quad (23)$$

The commutation relation, $[Q_{\text{ch}}, \mathcal{H}] = 0$, can be confirmed explicitly if we express eqs. (3)–(5) in terms of bonding and antibonding orbitals for $v_L = v_R$, and taking $t_{\nu,n}$ to be channel independent. The superconducting part, eq. (5), conserves the difference between the total number of the particles with the even symmetry and that of the odd ones,

$$\mathcal{H}_c^{\text{SC}} = \sum_{n=0}^{\infty} \Delta (a_{n\downarrow} b_{n\uparrow} + b_{n\downarrow} a_{n\uparrow} + b_{n\uparrow}^{\dagger} a_{n\downarrow}^{\dagger} + a_{n\uparrow}^{\dagger} b_{n\downarrow}^{\dagger}). \quad (24)$$

Here, Δ is real and defined such that $\Delta_R = -\Delta_L = \Delta$. The Hamiltonian can be simplified carrying out the particle-hole transformation for $b_{n\sigma}$,

$$g_{n\uparrow} = (-1)^{n+1} b_{n\downarrow}^{\dagger}, \quad g_{n\downarrow} = -(-1)^{n+1} b_{n\uparrow}^{\dagger}. \quad (25)$$

Then, the two leads consist a *normal* ladder

$$\mathcal{H}_c^0 = \sum_{n=0}^{\infty} \sum_{\sigma} t_n (a_{n+1\sigma}^{\dagger} a_{n\sigma} + g_{n+1\sigma}^{\dagger} g_{n\sigma} + \text{H.c.}), \quad (26)$$

$$\mathcal{H}_c^{\text{SC}} = \sum_{n=0}^{\infty} \sum_{\sigma} (-1)^{n+1} \Delta (a_{n\sigma}^{\dagger} g_{n\sigma} + g_{n\sigma}^{\dagger} a_{n\sigma}), \quad (27)$$

and one of the corners for $a_{0\sigma}$ is connected to the dot as $\mathcal{H}_T = \sum_{\sigma} \sqrt{2}v (a_{0\sigma}^{\dagger} d_{\sigma} + d_{\sigma}^{\dagger} a_{0\sigma})$. The dot part of the Hamiltonian, $\mathcal{H}_d^0 + \mathcal{H}_d^U$, keeps the original form given in eq. (2). Thus, it is obvious that the SC correlation vanishes, $\langle d_{\uparrow}^{\dagger} d_{\downarrow}^{\dagger} \rangle = 0$, at the impurity site in the present situation even for the particle-hole asymmetric case $\xi_d \neq 0$.

The ladder described by eqs. (26) and (27) gives the density of states that shows a square root divergence at the edges of the gap $\epsilon = \pm\Delta$. Therefore, the properties of the π -junction in the symmetric gaps and couplings must be essentially the same as those of the magnetic impurity in a band insulator, which has been studied using mainly a constant density of states with the gap around the Fermi level.^{26,27,28}

III. GROUND-STATE PROPERTIES

A. NRG approach

We study the ground-state properties using the NRG. In order to examine the effects caused by the asymmetry

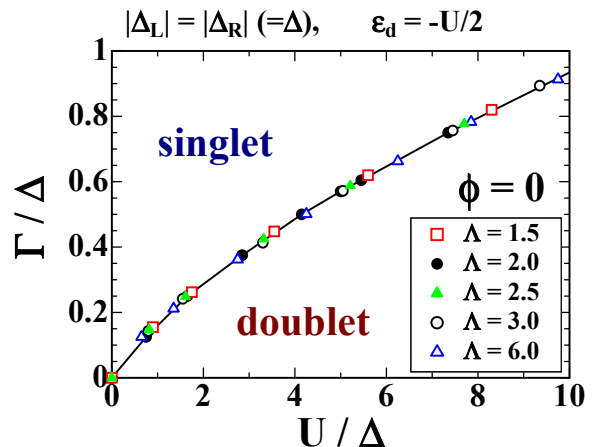


FIG. 3: Phase diagram of the ground state for $\phi = 0$ at half-filling $\epsilon_d = -U/2$ is plotted for several values of Λ : (\square) 1.5, (\bullet) 2.0, (\blacktriangle) 2.5, (\circ) 3.0, and (\triangle) 6.0, where $\Gamma_L = \Gamma_R (\equiv \Gamma)$, and $|\Delta_L| = |\Delta_R| (\equiv \Delta)$.

in the tunneling matrix elements, we consider the Josephson junction with $|\Delta_L| = |\Delta_R| (\equiv \Delta)$, where the two gaps are equal in size. To be specific, we assume that $\Gamma_{\nu}(\epsilon)$ is a constant inside the conduction band $-D < \epsilon < D$, and use the standard logarithmic discretization.³⁰ Then, the hopping and tunneling matrix elements are expressed in the form

$$t_{\nu,n} = D \frac{1 + 1/\Lambda}{2} \frac{(1 - 1/\Lambda^{n+1}) \Lambda^{-n/2}}{\sqrt{1 - 1/\Lambda^{2n+1}} \sqrt{1 - 1/\Lambda^{2n+3}}}, \quad (28)$$

$$v_{\nu} = \sqrt{\frac{2D \Gamma_{\nu} A_{\Lambda}}{\pi}}, \quad A_{\Lambda} = \frac{1}{2} \frac{1 + 1/\Lambda}{1 - 1/\Lambda} \log \Lambda. \quad (29)$$

The factor A_{Λ} is required for reproducing the original model correctly in the continuum limit $\Lambda \rightarrow 1$.^{30,31} We have carried out the successive diagonalizations of NRG keeping typically the lowest 500 energy states for constructing the Hilbert space with extra orbitals from next step. The low-energy properties are determined by the ratios Γ_{ν}/Δ , U/Δ , ϵ_d/Δ and the phase difference ϕ . In the calculations we have taken the gap to be $\Delta/D = 1.0 \times 10^{-5}$: this ratio itself does not affect the low-energy properties, provided $\Delta \ll D$. We have used the eigenvalue of the pseudo spin I_x as a quantum number to classify the Hilbert space in the particle-hole symmetric case for $\phi = 0$ and π . These two limits of ϕ provide the upper and lower bounds in the ground-state phase diagrams for intermediate ϕ .

The model for the Josephson junction contains two conduction bands, and the accuracy of the NRG results becomes somewhat worse than that for a single-channel model. For this reason, we have mainly used a rather large value $\Lambda = 6.0$ for the discretization parameter to get an early convergence in the NRG steps. To check the validity of it, we have examined the phase diagram of the

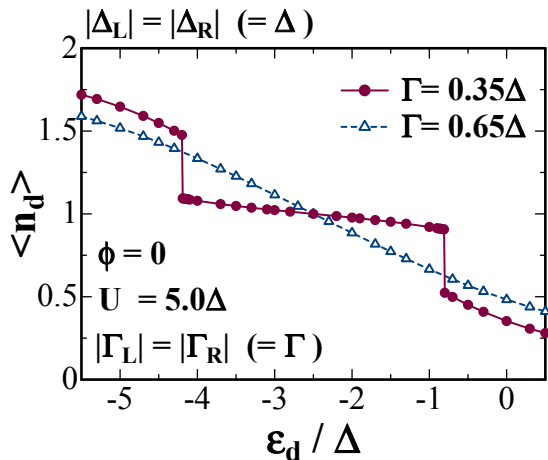


FIG. 4: Number of electrons in the dot $\langle n_d \rangle$ as a function of ϵ_d for $U = 5.0\Delta$, $|\Gamma_L| = |\Gamma_R| (\equiv \Gamma)$, and $|\Delta_L| = |\Delta_R| (\equiv \Delta)$. The ground state is a singlet for (\bullet) $\Gamma = 0.35\Delta$, while for (\triangle) $\Gamma = 0.65\Delta$ it changes to a doublet for $-4.2 \lesssim \epsilon_d \lesssim -0.8$. The discretization parameter is taken to be $\Lambda = 2.0$.

ground state changing the value of Λ ($= 1.5, 2.0, 2.5, 3.0$ and 6.0): we have preserved the lowest 2000 states for $\Lambda = 1.5$. The calculation has been carried out for $\phi = 0$ where the model can be reduced to a single-channel model, and the results obtained at half-filling $\epsilon_d = -U/2$ for the symmetric couplings $\Gamma_L = \Gamma_R (\equiv \Gamma)$ are shown in Fig. 3. We see that the results obtained at $\Lambda = 6.0$ already agree well with those obtained for small Λ 's. It indicates that the level crossing of the ground and first excited states is not so sensitive to Λ , and it supports the validity of our results presented in the following. The figure 3 itself shows that the ground state is a nonmagnetic singlet for large Γ or small U , and at the critical point it changes discontinuously to a magnetic doublet for small Γ or large U .^{8,25}

In order to show an example of the behavior of observables at the critical point, we have also calculated the average number of electrons $\langle n_d \rangle$ in the dot. The result is shown in Fig. 4 as a function of ϵ_d for $U = 5.0\Delta$, $\phi = 0$, and $\Gamma_L = \Gamma_R$. In this parameter set, the ground state for $\Gamma = 0.65\Delta$ is a singlet for all values of ϵ_d , and thus $\langle n_d \rangle$ decreases monotonically with increasing ϵ_d . In contrast, for $\Gamma = 0.35\Delta$, the ground state is a doublet for $-4.2 \lesssim \epsilon_d \lesssim -0.8$, and $\langle n_d \rangle$ jumps at the critical points. Other observable quantities, such as the Josephson current, will also show similar discontinuous changes, because the QPT between the singlet and double ground states is the first order transition occurring as a result of a level crossing of the Andreev bound state emerging in the SC gap in the energy spectrum.

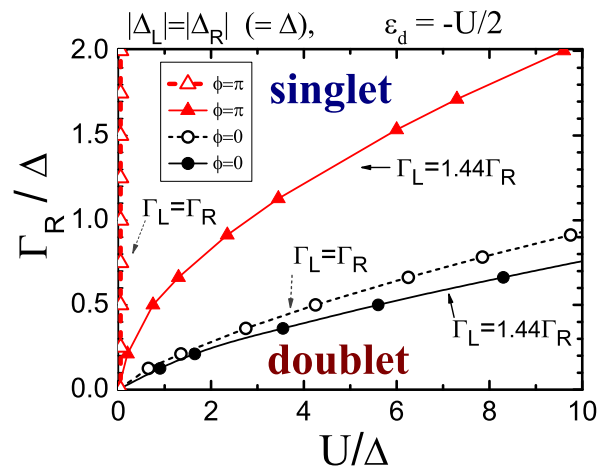


FIG. 5: Phase diagram of the ground state at half-filling $\epsilon_d = -U/2$ for asymmetric couplings $\Gamma_L = 1.44\Gamma_R$ with (\bullet) $\phi = 0$ and (\blacktriangle) $\phi = \pi$. The dashed lines show the phase boundaries for the symmetric couplings $\Gamma_L = \Gamma_R$ with (\circ) $\phi = 0$ and (\triangle) $\phi = \pi$. The SC gaps are taken to be $|\Delta_L| = |\Delta_R| (\equiv \Delta)$.

B. Asymmetric couplings $\Gamma_L \neq \Gamma_R$ at half-filling

How does the asymmetry in the couplings Γ_L and Γ_R affect the ground-state properties? We first of all consider the particle-hole symmetric case $\epsilon_d = -U/2$. In this case, the dot is occupied by a single electron $\langle n_d \rangle = 1$ on average, and magnetic correlations are enhanced maximally. In Fig. 5, the phase diagram of the ground state for asymmetric couplings $\Gamma_L = 1.44\Gamma_R$ is plotted for the Josephson junctions with (\bullet) $\phi = 0$ and (\blacktriangle) $\phi = \pi$. For comparison, the results obtained for the symmetric couplings $\Gamma_L = \Gamma_R$ are shown for (\circ) $\phi = 0$ and (\triangle) $\phi = \pi$ with the dashed lines. The phase boundary for intermediate values of ϕ , namely for $0 < \phi < \pi$, will appear in between the line for $\phi = 0$ and that for $\phi = \pi$. In the figure, we see a general trend that the phase difference ϕ between the SC pair potentials enlarges the region for a doublet ground state.²⁵ It means that the Josephson effects due to a finite ϕ disturbs the screening of the local moment, and the QPT will be driven by ϕ if the other parameters U/Δ and Γ_ν/Δ bring the system into the parameter region enclosed by the two lines. Note that for the data obtained for $\Gamma_L = 1.44\Gamma_R$, the sum of the hybridization energies $\Gamma_L + \Gamma_R$ is larger than that for the symmetric couplings. It also favors the singlet ground state.

The results shown in Fig. 5 suggest, however, that the superconducting proximity effects on the impurity site depends substantially on the asymmetry in the Josephson couplings, particularly for the π -junction. The vertical phase boundary at $\phi = \pi$ for $\Gamma_L = \Gamma_R$ is caused by an Andreev bound state. It emerges just on the Fermi level at half-filling, as we see also in the potential profile shown in Fig. 2 (b). Therefore, along the vertical line the ground

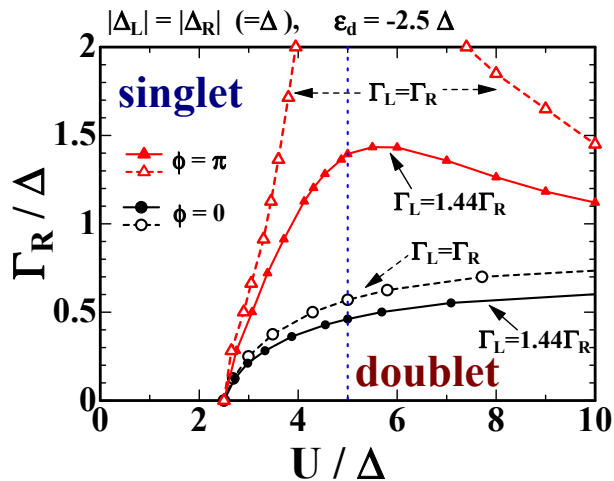


FIG. 6: Phase diagram of the ground state away from half-filling at $\epsilon_d = -2.5\Delta$ is plotted for asymmetric couplings $\Gamma_L = 1.44\Gamma_R$ for (\bullet) $\phi = 0$ and (\blacktriangle) $\phi = \pi$. Corresponding results for the symmetric couplings $\Gamma_L = \Gamma_R$ are also plotted for (\circ) $\phi = 0$ and (\triangle) $\phi = \pi$. Particle-hole symmetry holds at $U = 5.0\Delta$.

state has 4-fold degeneracy. An infinitesimal U lifts the degeneracy when the two SC gaps are identical $|\Delta_L| = |\Delta_R|$, and the ground state becomes a doublet in the whole region of $U > 0$. We will discuss this point more in detail in Sec. IV. The asymmetry in the couplings $\Gamma_L \neq \Gamma_R$ breaks this situation. Then, the Andreev bound state emerges away from the Fermi level, and it makes the ground state to be a singlet for small U .

C. Away from half-filling

We also consider the ground state away from half-filling $\epsilon_d \neq U/2$. The phase diagram obtained for a fixed value of the onsite energy $\epsilon_d = -2.5\Delta$ is shown in Fig. 6, where the particle-hole symmetry holds along the dashed line at $U = 5.0\Delta$. The calculations have been carried out for asymmetric couplings $\Gamma_L = 1.44\Gamma_R$ for (\bullet) $\phi = 0$ and (\blacktriangle) $\phi = \pi$, and also for the symmetric couplings $\Gamma_L = \Gamma_R$ for (\circ) $\phi = 0$ and (\triangle) $\phi = \pi$. As mentioned, the boundary for $0 < \phi < \pi$ will appear between the line for $\phi = 0$ and that for $\phi = \pi$. In Fig. 6, all the boundaries start from the point $U = 2.5\Delta$ in the horizontal axis. This is because in the atomic limit $\Gamma_\nu = 0$ the level crossing between the singlet and doublet states occurs at $2\epsilon_d + U = \epsilon_d$, when the energy of single-particle state and that of two-particle state coincide. We also see in this figure that the phase boundary for $\phi = \pi$ is changed substantially by the asymmetry in the couplings, and the parameter region corresponding to the singlet ground state spreads in an upper-right region for $\Gamma_R \gtrsim 1.4\Delta$ and $U \gtrsim 5.0\Delta$. For the symmetric couplings, the phase boundary at $\phi = \pi$ approaches asymptotically

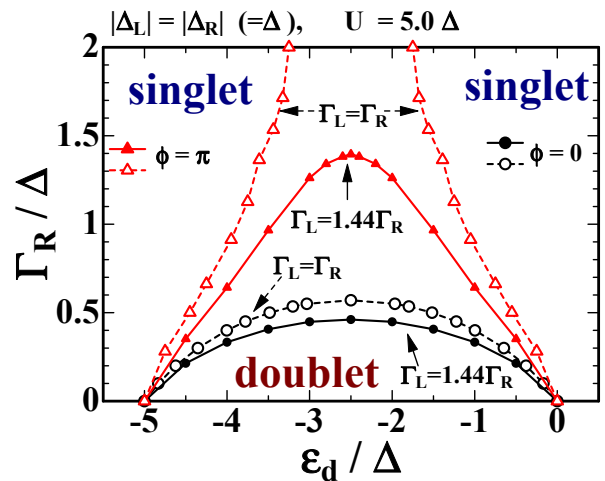


FIG. 7: Phase diagram of the ground state away from half-filling at $U = 5.0\Delta$ for asymmetric couplings $\Gamma_L = 1.44\Gamma_R$ for (\bullet) $\phi = 0$, (\blacktriangle) $\phi = \pi$, and the symmetric couplings $\Gamma_L = \Gamma_R$ for (\circ) $\phi = 0$, (\triangle) $\phi = \pi$. Particle-hole symmetry holds at $\epsilon_d = -2.5\Delta$.

to the vertical line at $U = 5.0\Delta$. This behavior is caused by the Andreev state approaching to the Fermi energy.

In quantum dots ϵ_d is a tunable parameter that can be controlled by the gate voltage. The ϵ_d dependence of the phase diagram of the ground state for $\Gamma_L = \Gamma_R$ has been obtained first with the slave-boson mean-field approximation by Rozhkov and Arovas.¹⁹ We have examined the effects of the asymmetry. The NRG results are shown in Fig. 7 for (solid line) the asymmetric couplings $\Gamma_L = 1.44\Gamma_R$, and for (dashed line) symmetric couplings $\Gamma_L = \Gamma_R$. Here, the Coulomb interaction is fixed to be $U = 5.0\Delta$. The ground state is a singlet for $\epsilon_d + U < 0$ and $\epsilon_d > 0$, because the impurity site is almost fully filled or almost empty in these two regions. We see again in Fig. 7 that the asymmetry in the couplings $\Gamma_L \neq \Gamma_R$ enlarges the parameter space of the singlet ground state. The phase boundary for $\phi = \pi$ in the symmetric couplings $\Gamma_L = \Gamma_R$ shows a diverging behavior at $\epsilon_d = -2.5\Delta$, which is owing to the Andreev bound state being situated just on the Fermi level at half-filling.

IV. DISCUSSIONS

The phase transition between the singlet and doublet ground states occurs at a level crossing of the lowest and the first many-body excited states, both of which are discrete and are separated from the continuous excitation spectrum at $\epsilon > \min(|\Delta_R|, |\Delta_L|)$ above the energy scale of the SC gap. Therefore, a few discrete states emerging inside the gap region determine the properties at low energy scales. In this section, to obtain some insights into how the asymmetry around the dot affects the ground states, we consider two simple limits where the model

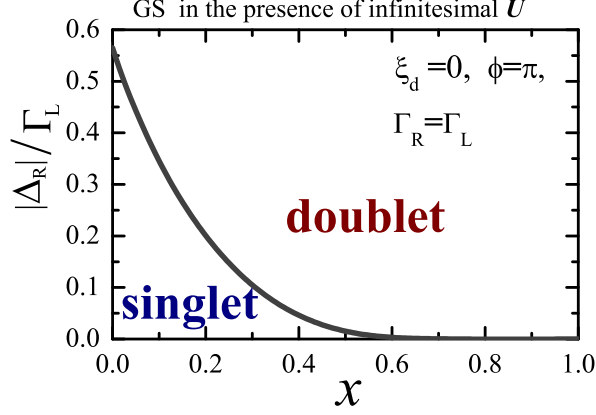


FIG. 8: Ground state for $\phi = \pi$, $\Gamma_R = \Gamma_L$, and $\xi_d = 0$ in the presence of an infinitesimal Coulomb interaction U , which lifts the degeneracy caused by the zero-energy Andreev state. Here, $x = |\Delta_R|/|\Delta_L|$, represents the asymmetry in the SC gaps, and $|\Delta_L|$ is changed in the region $|\Delta_L| > |\Delta_R|$ keeping $|\Delta_R|$ unchanged. The critical value of Γ at $x = 0$ is $\Gamma_{cr} \simeq 1.77|\Delta_R|$.

can be solved.

A. Noninteracting limit $\mathcal{H}_d^U = 0$

We consider here how the asymmetry in the two SC gaps affects the Andreev state in the noninteracting case $\mathcal{H}_d^U = 0$. The density of states of each SC lead has the square root divergence at the edge $\epsilon = \pm|\Delta_\nu|$, and the formation of the bound state depends strongly on these divergences. The edges are separated from each other for $|\Delta_R| \neq |\Delta_L|$, and they merge for the symmetric gaps to give a linear divergence for $0 < \phi \leq \pi$.

The energy of the Andreev state inside the gap is determined by an equation, $\det \{\mathbf{G}^0(\epsilon)\}^{-1} = 0$. The Green's function is defined in the appendix A. The explicit form of the determinant $F(\epsilon) \equiv \det \{\mathbf{G}^0(\epsilon)\}^{-1}$ is given, replacing the imaginary frequency $i\omega_n$ in eq. (A3) by the real one ϵ for $|\epsilon| < \min(|\Delta_R|, |\Delta_L|)$, as

$$F(\epsilon) = \epsilon^2 - \xi_d^2 - \Gamma_L^2 - \Gamma_R^2 + \frac{2\Gamma_L \epsilon^2}{\sqrt{|\Delta_L|^2 - \epsilon^2}} + \frac{2\Gamma_R \epsilon^2}{\sqrt{|\Delta_R|^2 - \epsilon^2}} + \frac{2\Gamma_L \Gamma_R (\epsilon^2 - |\Delta_L||\Delta_R| \cos \phi)}{\sqrt{|\Delta_L|^2 - \epsilon^2} \sqrt{|\Delta_R|^2 - \epsilon^2}}. \quad (30)$$

It takes a negative value, or vanishes, at $\epsilon = 0$,

$$F(0) = -\xi_d^2 - (\Gamma_R + \Gamma_L)^2 \cos^2 \frac{\phi}{2} - (\Gamma_R - \Gamma_L)^2 \sin^2 \frac{\phi}{2}. \quad (31)$$

Therefore, the bound state emerges if $F(\epsilon)$ increases with $|\epsilon|$ to reach zero. For $\pi/2 \leq \phi \leq \pi$, the solu-

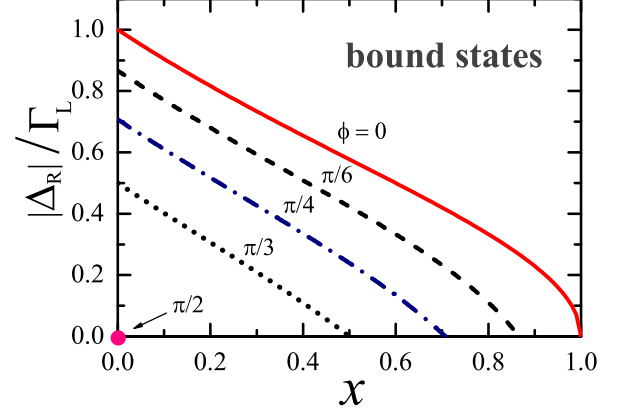


FIG. 9: Bound states for $U = 0$ exist in the region upside of each of the lines for $\phi = 0, \pi/6, \pi/4$, and $\pi/3$. For $\pi/2 < \phi \leq \pi$, the bound states always exist. Here, $x = |\Delta_R|/|\Delta_L|$, and $|\Delta_L|$ is changed in the region $|\Delta_L| > |\Delta_R|$ keeping $|\Delta_R|$ unchanged. The lines are determined by eq. (32), which does not depend on Γ_R nor ξ_d .

tion always exists because in this range of the phase $F(\epsilon)$ is an increasing function and diverges positively at $|\epsilon| = \min(|\Delta_R|, |\Delta_L|)$ with the square root dependence. Specifically, the bound state appears just on the Fermi level $\epsilon = 0$, when the right hand side of eq. (31) equals zero. It happens for $\xi_d = 0$, $\phi = \pi$, and $\Gamma_R = \Gamma_L$, provided $|\Delta_R|$ and $|\Delta_L|$ are nonzero. In this case the singlet and doublet ground states are degenerate because the energy does not depend on the way the bound state is occupied. The asymmetry in the couplings Γ_R and Γ_L affects crucially the ground-state property for the π -junction. The Coulomb interaction lifts the degeneracy, and it can be studied with a simple perturbation theory with respect to an infinitesimal U .²⁵ The results are shown in Fig. 8, assuming that $|\Delta_R| = \min(|\Delta_R|, |\Delta_L|)$. The way how the degeneracy is lifted depends quantitatively on the asymmetry in the SC gaps $x = |\Delta_R|/|\Delta_L|$. Specifically, the curve for the phase boundary reaches 0 at $x = 1$, which corresponds to the symmetric gaps $|\Delta_L| = |\Delta_R|$. It means that the ground state is a doublet for any values of Γ at $x = 1$. It explains the behavior of the vertical phase boundary for the π -junction in Fig. 5, and in this case the SC correlation in the impurity site vanishes $\langle d_\uparrow^\dagger d_\downarrow^\dagger \rangle = 0$ also for finite U as shown in the appendix A.

Another example seen in the case of asymmetric gaps $|\Delta_L| \neq |\Delta_R|$ is that the bound state disappears in a finite parameter region. It is caused by the difference in the asymptotic behavior $F(\epsilon)$ at $|\epsilon| \rightarrow |\Delta_R| - 0^+$, where we assume that $|\Delta_R| \leq |\Delta_L|$. For instance, in the limit of $|\Delta_L| \rightarrow \infty$, the determinant $F(\epsilon)$ does not have a zero point for $|\Delta_R| < \Gamma_L \cos \phi$.²⁵ This is because the SC correlation of the order Γ_L , which penetrates from left lead into the dot, pushed the bound state away towards the continuum outside of the gap region of the width

$|\Delta_R|$. The bound state can remain inside the gap for $|\Delta_R| > \Gamma_L \cos \phi$. The same situation also happens for finite $|\Delta_L|$. The existence of the bound state can be deduced from the asymptotic behavior of the determinant at the edge of the gap region. The bound states appears if $F(\epsilon) \rightarrow +\infty$ for $|\epsilon| \rightarrow |\Delta_R| - 0^+$, and this condition can be expressed in the form, for $0 \leq x < 1$ with $x = |\Delta_R|/|\Delta_L|$, as

$$\frac{|\Delta_R|}{\Gamma_L} > \frac{\cos \phi - x}{\sqrt{1-x^2}}. \quad (32)$$

The solution does not exist when the both sides of eq. (32) are equal, since $F(\epsilon)$ takes a negative finite value for $|\epsilon| \rightarrow |\Delta_R| - 0^+$ at the critical condition. The parameter region where the bound states do *not* exist shrinks as ϕ increases as shown in Fig. 9. In contrast, for the symmetric gaps $|\Delta_R| = |\Delta_L|$, the determinant shows a positive linear divergence for $0 < \phi \leq \pi$ at the edge of the gap, and the bound state always remains inside the gap region.

B. Large gap limit $|\Delta_R|, |\Delta_L| \rightarrow \infty$

When both of the two gaps $|\Delta_R|$ and $|\Delta_L|$ are larger than the other parameters, the model can be mapped onto a simple single site problem by taking a limit of $|\Delta_L| \rightarrow \infty$ and $|\Delta_R| \rightarrow \infty$.³² It can be regarded as a superconducting analogue of an atomic limit, and can be solved analytically as summarized in the appendix B. The properties in the symmetric couplings $\Gamma_R = \Gamma_L$ have been studied by Vecino *et al.*²¹ In the following, we discuss mainly the role of the asymmetry in the couplings $\Gamma_R \neq \Gamma_L$.

In the case of a normal transport through a quantum dot the equation of motion method,³³ which is essentially the atomic limit in the Hubbard I approximation,³⁴ has been applied to the properties at high energy scale. It has a limitation, however, at low temperatures because it does not describe properly the Fermi liquid properties due to the gapless low-energy excitations. Nevertheless, in the case of the dot connected to superconducting reservoirs, the low-energy excitations have the gap, and it gives a different meaning to the atomic limit. The single site degrees of freedom can be identified as the Andreev bound state remaining inside the gap. It does describe the lowest few many-body excited states inside the gap properly, and can also be considered as one of the fixed points of NRG. Although the virtual processes to the continuous excited states above the SC energy gap may also be important for the correlation functions, the main features of the contributions of the Andreev state to the low-energy properties, especially the bound-state energy itself, can be captured in the atomic limit of $|\Delta_L|, |\Delta_R| \rightarrow \infty$.

The effective Hamiltonian for the single site model is given in eq. (B4) in the appendix B. In the large gap limit, the role of the SC leads can be replaced by the SC

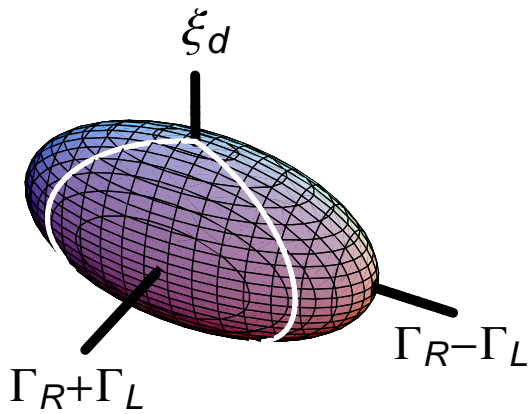


FIG. 10: Equi-energy surface of Andreev state E_A in a parameter space consisting of Γ_R , Γ_L , and ξ_d in the limit of $|\Delta_R|, |\Delta_L| \rightarrow \infty$. The phase ϕ changes the eccentricity of the ellipse in the horizontal plane, and the picture shows an example for a small ϕ ($\neq 0$). The central region between the two white longitudinal lines, which represent $\Gamma_R = 0$ and $\Gamma_L = 0$, is the physical parameter space for $\Gamma_\nu > 0$. The ground state is a doublet inside the surface which is determined such that $E_A = U/2$, and is a singlet for the outside.

pair potential at the impurity site $\Delta_d = \Gamma_L e^{i\theta_L} + \Gamma_R e^{i\theta_R}$, which is caused by the proximity effects. The energy of the Andreev state $E_A = \sqrt{\xi_d^2 + |\Delta_d|^2}$ given in (B5) can be rewritten in the form,

$$E_A = \sqrt{\xi_d^2 + (\Gamma_R + \Gamma_L)^2 \cos^2 \frac{\phi}{2} + (\Gamma_R - \Gamma_L)^2 \sin^2 \frac{\phi}{2}}. \quad (33)$$

Therefore, the equi-energy surface of E_A can be described as an ellipsoid in a three-dimensional space consisting of ξ_d and $\Gamma_R \pm \Gamma_L$ as shown in Fig. 10. The Josephson phase ϕ changes the aspect ratio, or eccentricity, of the ellipsoid. Specifically, for $\phi \simeq \pi$, the gradient along the $\Gamma_R - \Gamma_L$ axis becomes large, and it implies that the asymmetry in the coupling plays an important role on the properties near the π -junction.

The ground state is a doublet for $E_A < U/2$, and it is a singlet for $E_A > U/2$. Therefore, the Coulomb interaction determines the size of an ellipsoidal such that

$$E_A = U/2. \quad (34)$$

The inside corresponds to a doublet ground state, and the outside is a singlet. The equations (33) and (34) explain the features of the phase diagrams, shown in Figs. 5–7, for small parameter values, at $\max(\Gamma_R, \Gamma_L, U, |\xi_d|) \ll \Delta$. Particularly, Fig. 7 can be related to a cross section of the ellipsoid for a fixed $U/2$. For instance, for $\phi = \pi$, the phase diagram in the atomic limit is determined by $\xi_d^2 + (\Gamma_R - \Gamma_L)^2 = U^2/4$, and thus the phase boundary becomes two open sheets at $\xi_d = \pm U/2$ for the symmetric couplings $\Gamma_R = \Gamma_L$, while the asymmetry $\Gamma_R \neq \Gamma_L$ closes the sheets to form an elliptic cylinder. As another simple

example, we consider the symmetric couplings $\Gamma_R = \Gamma_L$ ($\equiv \Gamma$), for which the boundary is given by $4\Gamma^2 \cos^2 \frac{\phi}{2} = U^2/4 - \xi_d^2$. This equation corresponds to the dashed lines shown in Figs. 5 and 6 for small Γ .

In the atomic limit the first and second many-body excitation energies E_1 and E_2 , measured from the ground-state energy, are given by

$$\text{singlet GS: } \begin{cases} E_1 = E_A - U/2 \\ E_2 = 2E_A \end{cases} \quad \text{for } E_A > \frac{U}{2}, \quad (35)$$

$$\text{doublet GS: } \begin{cases} E_1 = U/2 - E_A \\ E_2 = U/2 + E_A \end{cases} \quad \text{for } E_A < \frac{U}{2}. \quad (36)$$

Two discrete many-body excited states can appear in the energy gap even for finite SC gaps, for which the energies can be calculated with NRG. Then, eqs. (35) and (36) could be used to determine the renormalized values of U and E_A , which asymptotically coincide with the bare ones in the limit of $|\Delta_L|, |\Delta_R| \rightarrow \infty$. The renormalization is caused by the contribution of the continuous states above the energy gap. The analysis of the fixed point along these lines will be discussed elsewhere.

V. SUMMARY

We have studied effects of the asymmetry in the Josephson couplings $\Gamma_L \neq \Gamma_R$ on the ground state of a quantum dot embedded between two superconductors. Specifically, we have obtained the phase diagram of the ground state in some parameter regions. The results show that the asymmetry in the couplings enhances the screening of the local moment in the dot, particularly for the π junction. For $\phi \simeq \pi$, the Andreev bound state emerges near the Fermi level in the symmetric couplings $\Gamma_L = \Gamma_R$, and it favors the magnetic doublet ground state for $U > 0$. The asymmetry in the couplings moves the Andreev bound state away from the Fermi level, and enhances the screening of the local moment. The boundary between the singlet and doublet ground states for intermediate phase $0 < \phi < \pi$ must be in between the curves for $\phi = 0$ and that for $\phi = \pi$.

We have also described some symmetry properties of the Anderson impurity in the Josephson junction in terms of the spinor rotation in the pseudo-spin and the current conservation. Specifically, the similarity between the π -junction and a magnetic impurity in an insulating host has been discussed based on a symmetry property. Furthermore, the role of the asymmetry in the couplings and gaps has been discussed in the noninteracting case, and also in the limit of $|\Delta_L|, |\Delta_R| \rightarrow \infty$. Our results suggest that in real quantum dots the ground-state properties depends in various ways on the local conditions surrounding the dot.

Acknowledgements

We would like to thank Yoichi Tanaka, Y. Nisikawa, and J. Bauer for valuable discussions. One of us (AO) is supported by the Grant-in-Aid for Scientific Research from JSPS. ACH wishes to thank the EPSRC (Grant GR/S18571/01) for financial support. Numerical computation was partly carried out at the computation center of Yukawa Institute.

APPENDIX A: CURRENT CONSERVATION

The imaginary-time Green's function for the Anderson impurity in the SC hosts can be described in the Nambu representation as

$$\mathbf{G}(i\omega_n) = -\int_0^\beta d\tau e^{i\omega_n\tau} \begin{bmatrix} \langle T_\tau d_\uparrow(\tau) d_\uparrow^\dagger \rangle & \langle T_\tau d_\uparrow(\tau) d_\downarrow \rangle \\ \langle T_\tau d_\downarrow^\dagger(\tau) d_\uparrow^\dagger \rangle & \langle T_\tau d_\downarrow^\dagger(\tau) d_\downarrow \rangle \end{bmatrix}, \quad (A1)$$

where $\omega_n = (2n+1)\pi/\beta$ for $n = 0, \pm 1, \pm 2, \dots$, $\beta = 1/T$, and T the temperature. The Dyson equation is given by

$$\{\mathbf{G}(i\omega_n)\}^{-1} = \{\mathbf{G}^0(i\omega_n)\}^{-1} - \mathbf{\Sigma}(i\omega_n), \quad (A2)$$

where $\mathbf{\Sigma}(i\omega_n)$ is the self-energy caused by \mathcal{H}_d^U , and

$$\{\mathbf{G}^0(i\omega_n)\}^{-1} = i\omega_n \mathbf{1} - \xi_d \tau_3 + \sum_{\nu=L,R} \Gamma_\nu \frac{i\omega_n \mathbf{1} - \Delta_\nu}{\sqrt{\omega_n^2 + |\Delta_\nu|^2}}. \quad (A3)$$

The currents through the dot is defined based on the Heisenberg equation, $\partial n_d / \partial t = (-i/\hbar)[n_d, \mathcal{H}]$, as

$$e \frac{\partial n_d}{\partial t} + J_R - J_L = 0, \quad (A4)$$

$$J_R = -i \frac{e v_R}{\hbar} \sum_\sigma \left(c_{R,0\sigma}^\dagger d_\sigma - d_\sigma^\dagger c_{R,0\sigma} \right), \quad (A5)$$

$$J_L = -i \frac{e v_L}{\hbar} \sum_\sigma \left(d_\sigma^\dagger c_{L,0\sigma} - c_{L,0\sigma}^\dagger d_\sigma \right). \quad (A6)$$

Here, J_L is the current flowing into the dot from the left, J_R is the current from the dot to the right. The thermal average of these currents can be expressed in terms of the Green's function

$$\langle J_R \rangle = \frac{2e}{\hbar\beta} \sum_{\omega_n} \frac{i\Gamma_R}{\sqrt{\omega_n^2 + |\Delta_R|^2}} \text{Tr} \left[\tau_3 \Delta_R \mathbf{G}(i\omega_n) \right], \quad (A7)$$

$$\langle J_L \rangle = \frac{2e}{\hbar\beta} \sum_{\omega_n} \frac{-i\Gamma_L}{\sqrt{\omega_n^2 + |\Delta_L|^2}} \text{Tr} \left[\tau_3 \Delta_L \mathbf{G}(i\omega_n) \right]. \quad (A8)$$

Here, the trace is taken over for the 2×2 matrices for the pseudo spin space. The current conservation $\langle J_L \rangle = \langle J_R \rangle$ indicates that there is one relation between the off diagonal elements of $\mathbf{G}(i\omega_n)$. For instance, the self-energy matrix can be described by three functions $a_0(i\omega_n)$, $a_3(i\omega_n)$,

and $a_{\alpha\delta;\lambda\rho}^\perp(i\omega_n, i\omega_m)$:

$$\Sigma(i\omega_n) = a_0(i\omega_n) i\omega_n \mathbf{1} + a_3(i\omega_n) \xi_d \boldsymbol{\tau}_3 + \Sigma_\perp(i\omega_n), \quad (\text{A9})$$

$$\left\{ \Sigma_\perp(i\omega_n) \right\}_{\alpha\delta} = \frac{1}{\beta} \sum_{i\omega_m} \sum_{\lambda,\rho} a_{\alpha\delta;\lambda\rho}^\perp(i\omega_n, i\omega_m) \times \left\{ \frac{\Gamma_L \Delta_L}{\sqrt{\omega_n^2 + |\Delta_L|^2}} + \frac{\Gamma_R \Delta_R}{\sqrt{\omega_n^2 + |\Delta_R|^2}} \right\}_{\rho\lambda}. \quad (\text{A10})$$

The kernel $a_{\alpha\delta;\lambda\rho}^\perp(i\omega_n, i\omega_m)$ for the off-diagonal part of the self-energy $\Sigma_\perp(i\omega_n)$ can be shown, using a Ward-Takahashi identity,³⁵ to be expressed in the form,

$$a_{\alpha\delta;\lambda\rho}^\perp(i\omega_n, i\omega_m) = \sum_{\mu_4} \sum_{\mu_2, \mu_3} \{ \boldsymbol{\tau}_3 \}_{\alpha\mu_4} \Gamma_{\mu_4\delta;\mu_2\mu_3}(i\omega_n, i\omega_n; i\omega_m, i\omega_m) \times \left\{ \mathbf{G}(i\omega_m) \boldsymbol{\tau}_3 \right\}_{\mu_3\rho} \left\{ \mathbf{G}(i\omega_m) \right\}_{\lambda\mu_2}. \quad (\text{A11})$$

Here, $\Gamma_{\mu_4\mu_1;\mu_2\mu_3}(i\omega_4, i\omega_1; i\omega_2, i\omega_3)$ is the vertex function in the Nambu representation, and μ_j ($j = 1, 2, 3, 4$) represents the component of the pseudo spins. From these properties, it is deduced that, if the both couplings and gaps are symmetric $\Gamma_R = \Gamma_L$ ($\equiv \Gamma$) and $|\Delta_R| = |\Delta_L|$ ($\equiv \Delta$) for the π -junction $\phi = \pi$, the off diagonal part of the self-energy vanishes at the impurity site. It simplifies the Green's function as

$$\left\{ \mathbf{G}(i\omega_n) \right\}^{-1} \Rightarrow i\omega_n \left(1 + \frac{2\Gamma}{\sqrt{\omega_n^2 + \Delta^2}} - a_0(i\omega_n) \right) \mathbf{1} - \left(1 + a_3(i\omega_n) \right) \xi_d \boldsymbol{\tau}_3. \quad (\text{A12})$$

Therefore, in this particular case the SC correlation cancels out in the impurity site $\langle d_\uparrow^\dagger d_\uparrow^\dagger \rangle = 0$, as can be deduced from eq. (A1). Furthermore, if the system also has the particle-hole symmetry $\xi_d = 0$ additionally, the Green's function is simply proportional to the unit matrix $\mathbf{1}$.

APPENDIX B: LIMIT OF $|\Delta_R|, |\Delta_L| \rightarrow \infty$

In the limit of $|\Delta_L| \rightarrow \infty$ and $|\Delta_R| \rightarrow \infty$, the model can be mapped onto a simple single-site problem,^{21,25,32} which can be solved analytically. In this limit, the Dyson equation eq. (A2) can be rewritten in the form

$$\left\{ \mathbf{G}^\infty(i\omega_n) \right\}^{-1} = i\omega_n \mathbf{1} - \mathbf{H}_d^0 - \Sigma^\infty(i\omega_n), \quad (\text{B1})$$

$$\mathbf{H}_d^0 = \begin{bmatrix} \xi_d & \Delta_d \\ \Delta_d^* & -\xi_d \end{bmatrix}, \quad \Delta_d = \Gamma_L e^{i\theta_L} + \Gamma_R e^{i\theta_R}. \quad (\text{B2})$$

The SC correlation penetrates into the dot from the SC leads via Γ_L and Γ_R . Therefore, the amplitude depends on the Josephson phase $\phi = \theta_R - \theta_L$,

$$|\Delta_d|^2 = (\Gamma_R + \Gamma_L)^2 - 4\Gamma_R\Gamma_L \sin^2 \frac{\phi}{2}. \quad (\text{B3})$$

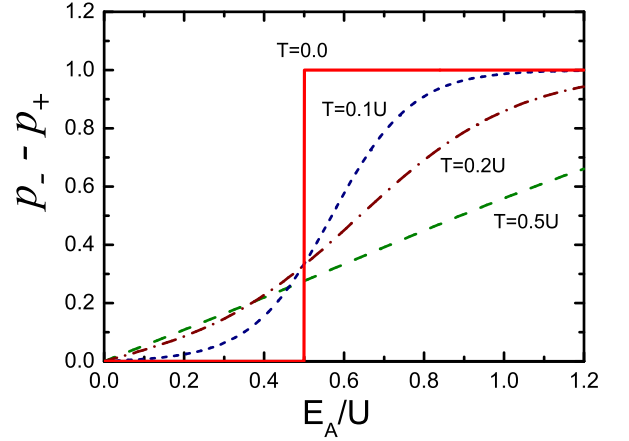


FIG. 11: Statistical weight $p_- - p_+$ as a function of E_A for $T/U = 0.0, 0.1, 0.2,$ and 0.5 .

The corresponding single-site Hamiltonian is given by

$$\mathcal{H}^\infty = \boldsymbol{\psi}_d^\dagger \mathbf{H}_d^0 \boldsymbol{\psi}_d + \frac{2U}{3} \vec{i}_d \cdot \vec{i}_d. \quad (\text{B4})$$

The noninteracting part determines the energy scale of the Andreev bound state $E_A \equiv \sqrt{\xi_d^2 + |\Delta_d|^2}$. The ground state is a singlet for $E_A > U/2$, while it is a doublet for $E_A < U/2$. The boundary between these two ground states is determined by the equation $U/2 = E_A$. Since the bound-state energy E_A depends on $\phi = \theta_R - \theta_L$ as

$$E_A = \sqrt{\xi_d^2 + (\Gamma_R + \Gamma_L)^2 - 4\Gamma_R\Gamma_L \sin^2 \frac{\phi}{2}}, \quad (\text{B5})$$

the phase transition occurs in between $0 < \phi < \pi$, if the Coulomb interaction is in the region $E_{A\pi} < U/2 < E_{A0}$. Here, $E_{A0,\pi}$ is the value of E_A at $\phi = 0, \pi$.

The Green's function can be obtained analytically

$$\mathbf{G}^\infty(i\omega_n) = \sum_{\eta=+,-} p_\eta \frac{i\omega_n \mathbf{1} + (1 + \eta \frac{U}{2E_A}) \mathbf{H}_d^0}{(i\omega_n)^2 - (\frac{U}{2} + \eta E_A)^2}, \quad (\text{B6})$$

$$p_\pm = \frac{1 + e^{-\beta(\frac{U}{2} \pm E_A)}}{2 + e^{-\beta(\frac{U}{2} + E_A)} + e^{-\beta(\frac{U}{2} - E_A)}}. \quad (\text{B7})$$

The equal time correlations, $\mathbf{G}(\tau)|_{\tau \rightarrow -0+}$, is given by

$$\begin{bmatrix} \langle d_\uparrow^\dagger d_\uparrow \rangle & \langle d_\downarrow d_\uparrow \rangle \\ \langle d_\uparrow^\dagger d_\downarrow \rangle & \langle d_\downarrow d_\downarrow \rangle \end{bmatrix} = \frac{1}{2} \mathbf{1} + \frac{p_- - p_+}{2E_A} \mathbf{H}_d^0. \quad (\text{B8})$$

Note that in the noninteracting case $U = 0$, the statistical weight $p_- - p_+$ is replaced by $1 - 2f(E_A)$ with $f(\epsilon) = [e^{\beta\epsilon} + 1]^{-1}$. In Fig. 11, the weight $p_- - p_+$ is plotted as a function of E_A/U for several temperatures. Specifically at zero temperature, $p_- = 1$ and $p_+ = 0$, for $E_A > U/2$ in the singlet ground state. It takes the value $p_- = p_+ =$

$1/2$ for $E_A < U/2$ in the doublet ground state. Therefore, at $T = 0$, the self-energy can be expressed in the form

$$\Sigma^\infty(i\omega) = \begin{cases} -\frac{U}{2E_A} \mathbf{H}_d^0 & , \quad E_A > \frac{U}{2} \\ \frac{U^2}{4} \frac{i\omega \mathbf{1} + \mathbf{H}_d^0}{(i\omega)^2 - E_A^2} & , \quad E_A < \frac{U}{2} \end{cases} . \quad (\text{B9})$$

The Josephson current can be calculated substituting eq. (B6) into eq. (A7) or (A8),

$$\langle J \rangle = \frac{e}{\hbar} \frac{p_- - p_+}{2E_A} 4\Gamma_R \Gamma_L \sin \phi . \quad (\text{B10})$$

At $T = 0$, the current can be expressed in the form

$$\langle J \rangle = \begin{cases} \frac{eE_{A0}}{\hbar} \frac{\mathcal{T} \sin \phi}{2\sqrt{1 - \mathcal{T} \sin^2 \frac{\phi}{2}}} & , \quad E_A > \frac{U}{2} \\ 0 & , \quad E_A < \frac{U}{2} \end{cases} . \quad (\text{B11})$$

where $E_{A0} = \sqrt{\xi_d^2 + (\Gamma_R + \Gamma_L)^2}$ is the maximum value of the bound-state energy, and $\mathcal{T} \equiv 4\Gamma_R \Gamma_L / E_{A0}^2$ corresponds to a normal transmission probability for non-interacting electrons. The contribution of the Coulomb interaction disappears at $T = 0$ in the case of the singlet ground state as discussed by Glazman and Matveev.¹⁰ The Josephson current vanishes for the magnetic doublet ground state in the limit of $|\Delta_R|, |\Delta_L| \rightarrow \infty$. A finite current flowing in the opposite direction in the case of the finite SC gaps,³ is caused by the continuous excited states above the gaps.

-
- ¹ T. Soda, T. Matsuura, and Y. Nagaoka, *Prog. Theor. Phys.* **38**, 551 (1967).
² T. Matsuura, *Prog. Theor. Phys.* **57**, 1823 (1977).
³ H. Shiba and T. Soda, *Prog. Theor. Phys.* **41**, 25 (1969).
⁴ E. Müller-Hartman and J. Zittartz, *Z. Phys.* **234**, 58 (1970).
⁵ M. Jarrell, D. S. Sivia and B. Patton, *Phys. Rev. B* **42**, 4804 (1990).
⁶ K. Satori, H. Shiba, O. Sakai, and Y. Shimizu, *J. Phys. Soc. Jpn.* **61**, 3239 (1992).
⁷ O. Sakai, Y. Shimizu, H. Shiba, and K. Satori, *J. Phys. Soc. Jpn.* **62**, 3181 (1993).
⁸ T. Yoshioka and Y. Ohashi, *J. Phys. Soc. Jpn.* **69**, 1812 (2000).
⁹ M. Matsumoto and M. Koga, *J. Phys. Soc. Jpn.* **70**, 2860 (2001).
¹⁰ L. I. Glazman and K. A. Matveev, *Pis'ma Zh. Eksp. Teor. Fiz.* **49** (1989) 570 [*JETP Lett.* **49** (1989) 659].
¹¹ B. I. Spivak and S. A. Kivelson, *Phys. Rev. B* **43** (1991) 3740.
¹² C. W. J. Beenakker, in *Transport Phenomena in Mesoscopic Systems*, edited by H. Fukuyama and T. Ando (Springer-Verlag, Berlin, 1992).
¹³ M. R. Buitelaar, T. Nussbaumer and C. Schönberger, *Phys. Rev. Lett.* **89**, 256801 (2002).
¹⁴ M. R. Buitelaar, W. Belzig, T. Nussbaumer, B. Babić, C. Bruder, and C. Schönberger, *Phys. Rev. Lett.* **91**, 057005 (2003).
¹⁵ J. A. van Dam, Yuli V. Nazarov, Erik P. A. M. Bakkers, S. De Franceschi, L. P. Kouwenhoven, *Nature* **442**, 667 (2006).
¹⁶ J.-P. Cleuziou, W. Wernsdorfer, V. Bouchiat, Th. Ondarcuhu, M. Monthieux, *cond-mat/0610622*.
¹⁷ S. Ishizaka, J. Sone, and T. Ando, *Phys. Rev. B* **52**, 8358 (1995).
¹⁸ A. A. Clerk and V. Ambegaokar, *Phys. Rev. B* **61**, 9109 (2000).
¹⁹ A. V. Rozhkov and D. P. Arovas, *Phys. Rev. Lett.* **82**, 2788 (1999).
²⁰ Y. Avishai, A. Golub and A. D. Zaikin, *Phys. Rev. B* **67**, 041301 (2003).
²¹ E. Vecino, A. Martin-Rodero, and A. Levy Yeyati, *Phys. Rev. B* **68**, 035105 (2003).
²² F. Siano and R. Egger, *Phys. Rev. Lett.* **93**, 047002 (2004).
²³ K. Kusakabe, Y. Tanaka, and Y. Tanuma, *Physica E*, **18**, 50 (2003).
²⁴ M.-S. Choi, M. Lee, K. Kang, and W. Belzig, *Phys. Rev. B* **70**, 020502 (2004).
²⁵ A. Oguri, Y. Tanaka, and A.C. Hewson, *J. Phys. Soc. Jpn.* **73**, 2494 (2004).
²⁶ J. Ogura and T. Saso, *J. Phys. Soc. Jpn.* **62**, 4364 (1993).
²⁷ K. Takegahara, Y. Shimizu, and O. Sakai, *J. Phys. Soc. Jpn.* **61**, 3443 (1992).
²⁸ K. Chen and C. Jayaprakash, *Phys. Rev. B* **57**, 5225 (1998).
²⁹ A. C. Hewson, *The Kondo Problem to Heavy Fermions* (Cambridge University Press, Cambridge, 1993).
³⁰ H. R. Krishna-murthy, J. W. Wilkins, and K. G. Wilson, *Phys. Rev. B* **21**, 1003 (1980).
³¹ O. Sakai, Y. Shimizu, and T. Kasuya, *Prog. Theor. Phys. Suppl.* **108**, 73 (1992).
³² I. Affleck, J. -S. Caux, and A. M. Zagoskin, *Phys. Rev. B* **62** 1433, (2000).
³³ Y. Meir, N. S. Wingreen, and P. A. Lee, *Phys. Rev. Lett.* **66**, 3048 (1991).
³⁴ J. Hubbard, *Proc. Roy. Soc. A*, **276**, 238 (1963).
³⁵ A. Oguri, unpublished.